Title

Visualization of cardiac thick filament dynamics in ex vivo heart preparations.

Authors

Kelly, Colleen

Martin, Jody

Coseno, Molly

et al.

Publication Date

2023-12-01

DOI

10.1016/j.yjmcc.2023.10.013

Peer reviewed

HHS Public Access

Author manuscript

J Mol Cell Cardiol. Author manuscript; available in PMC 2024 December 01.

Published in final edited form as:

J Mol Cell Cardiol. 2023 December ; 185: 88–98. doi:10.1016/j.yjmcc.2023.10.013.

Visualization of Cardiac Thick Filament Dynamics in *ex vivo* Heart Preparations

Colleen M. Kelly[1], **Jody L. Martin**[2], **Molly Coseno**[3], **Michael J. Previs**[1,†]

[1]Molecular Physiology and Biophysics Department, University of Vermont, Larner College of Medicine, Burlington, VT 05405

[2]Department of Pharmacology, University of California, Davis, Davis, CA 90095

[3]Fluidic Analytics, The Paddocks Business Centre, Cambridge, United Kingdom CB1 8DH

Abstract

Rationale—Cardiac muscle cells are terminally differentiated after birth and must beat continually throughout one's lifetime. This mechanical process is driven by the sliding of actin-based thin filaments along myosin-based thick filaments, organized within sarcomeres. Despite costly energetic demand, the half-life of the proteins that comprise the cardiac thick filaments is ~10 days, with individual molecules being replaced stochastically, by unknown mechanisms.

Objectives—To allow for the stochastic replacement of molecules, we hypothesized that the structure of thick filaments must be highly dynamic *in vivo*.

Methods and Results—To test this hypothesis in adult mouse hearts, we replaced a fraction of the endogenous myosin regulatory light chain (RLC), a component of thick filaments, with GFP-labeled RLC by adeno-associated viral (AAV) transduction. The RLC-GFP was properly localized to the heads of the myosin molecules within thick filaments in *ex vivo* heart preparations and had no effect on heart size or actin filament siding *in vitro*. However, the localization of the RLC-GFP molecules was highly mobile, changing its position within the sarcomere on the minute timescale, when quantified by fluorescence recovery after photobleaching (FRAP) using multiphoton microscopy. Interestingly, RLC-GFP mobility was restricted to within the boundaries of single sarcomeres. When cardiomyocytes were lysed, the RLC-GFP remained strongly bound to myosin heavy chain, and the intact myosin molecules adopted a folded, compact configuration, when disassociated from the filaments at physiological ionic conditions.

Conclusions—These data demonstrate that the structure of the thick filament is highly dynamic in the intact heart, with a rate of molecular exchange into and out of thick filaments that is

[†]**Corresponding Author:** Michael J. Previs, University of Vermont, Dept. of Molecular Physiology & Biophysics, Health Science Research Facility, 149 Beaumont Avenue, HSRF 108, Burlington, VT 05405-0075 USA, michael.previs@med.uvm.edu.

Disclosures

The authors have no competing interests to declare.

~1,500 times faster than that required for the replacement of molecules through protein synthesis or degradation.

Graphical Abstract

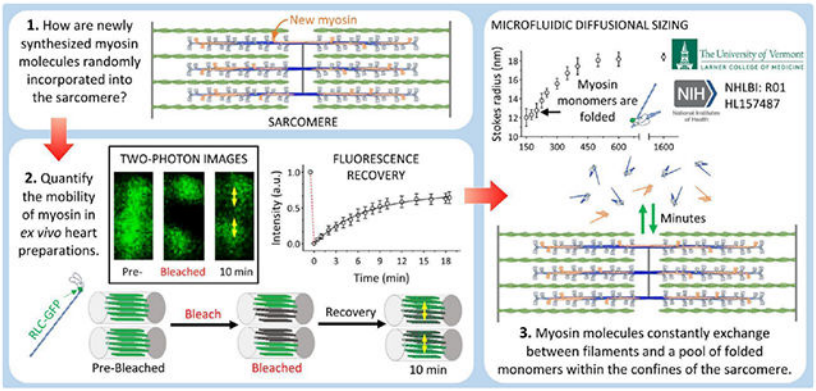

1. Introduction

Cardiac muscle cells are terminally differentiated after birth [1] and beat continuously throughout one's lifetime due to the coordinated contraction of sarcomeres, located within myofibrils. In an adult mouse heart, each sarcomere must contract ~500 times per minute to meet metabolic demands. These contractions require myosin molecules, organized in bipolar thick filaments, to bind actin molecules, organized in interdigitated thin filaments (Fig. 1A). Due to the importance of these mechanical interactions for cellular and whole heart function, thick filaments appear to maintain their structural and functional integrity by continually replacing their components through protein synthesis and degradation [2–3]. However, the mechanism(s) by which this replacement occurs, while the sarcomere continues to maintain its contractile function are largely unknown.

Myosin molecules are the most abundant protein complexes in the heart representing 4.3% of the total mass [4]. Each myosin molecule is a 520-kDa hexamer consisting of two heavy chains and four light chains. The N-terminus of each heavy chain forms a globular head decorated with an essential (ELC) and regulatory light chain (RLC) (Fig. 1B). These light chains play critical roles in maintaining the structural integrity of the head, and transmission of forces generated when myosin is bound to actin [5]. The central and C-terminal regions of the two heavy chains dimerize into a long coiled-coil, to form a single myosin molecule [6].

Approximately 300 myosin molecules copolymerize through intermolecular electrostatic interactions between the coiled-coil tails [7–10] to form each bipolar thick filament (Fig. 1A). We have recently demonstrated that cardiac muscle cells within adult mouse hearts constantly synthesize new myosin molecules, and these molecules randomly replace those within preexisting thick filaments [11]. This results in the average half-life of a myosin molecule being ~10 days *in vivo* [11]. This high rate of myosin replacement implies structural dynamics, which are at odds with elegant studies that demonstrate the structure of individual thick filaments is highly organized when imaged with electron microscopy [12, 13]. Yet, *in vitro* assays suggest that the electrostatic interactions between myosin

tails are transient [14–17], which could allow for the exchange of molecules between the filaments and a small pool of monomers. Moreover, cellular studies demonstrate the molecular machineries and transcripts required for thick filament protein synthesis and degradation are located at the boundaries of individual sarcomeres, rather than in some distal portion of the cell [18, 19]. Taken together, these data support the hypothesis that new myosin molecules are translated within the sarcomere and the molecules are randomly exchanged into and out of the thick filaments on an undefined timescale.

To determine whether such exchange happens in an intact heart, and to define the temporal and spatial aspects of these processes, we replaced a fraction of the endogenous cardiac myosin regulatory light chain (RLC) in adult mice, with RLC having green fluorescent protein (GFP) fused to its C-terminus (RLC-GFP). We visualized the localization and mobility of these molecules in *ex vivo* heart preparations using two-photon confocal imaging coupled with fluorescence recovery after photobleaching (FRAP). To determine whether the RLC-GFP remained bound to the myosin heavy chain when disassociated from the thick filaments, we lysed the cells and used a combination of biochemical and biophysical assays to quantify the abundance of soluble myosin and determine the Stokes radius of the GFP-labeled molecules in the soluble fraction. Together, these data demonstrate that the structure of the thick filament is highly dynamic in the adult heart, with individual molecules rapidly exchanging between thick filaments and a soluble pool of monomers. Unexpectedly, the rate of this exchange is ~1,500 times faster in *ex vivo* heart preparations, than that required for the replacement of the molecules by protein synthesis and degradation *in vivo*. These data suggest thick filaments are designed in such a way to allow for the constant exchange of their structural components to facilitate their replacement. We propose that these features may be key to molecular housekeeping that ensures contractile fidelity.

2. Methods

2.1. Animals

FVB-strain mice were obtained from Jackson Laboratory. Mice were cared for and euthanized in accordance with protocols approved by the University of Vermont Animal Care and Use Committee.

2.2. AAV design, production and use

Mouse MLC2v was fused in frame with pENN.AAV.cTNT.PI.eGFP.WPRE.rBG which was a gift from James M. Wilson (Addgene viral prep # 105543-AAV9; http://n2t.net/addgene:105543; RRID:Addgene_105543). To construct recombinant chimera, AAV9/pENN.AAV.cTNT.MLCV2.eGFP.WPRE.rBG was co-transfected along with pAAV2/9.45- (serotype 2 rep coding sequences, serotype 9.45 cap coding sequences) and pHelper plasmids (Stratagene) into AAV-293 cells utilizing PEI. The transfected cells were incubated for 72 hours before the cells were collected and subjected to 3 freeze-thaw cycles and benzonase treatment. After clarification, the supernatant was overlaid on iodixanol step gradient of 60%, 40%, 25% and 15% iodixanol in a quick-seal tube. Ultracentrifugation was carried out at 500,000 xg (70,000 RPM, 1 hour). The 60-40 interface was collected

(containing the live virus particles) and centrifugally dialyzed and concentrated to appropriate volumes. AAV stocks were titered for vector genomes by slot blotting (psoralen-biotin and Brightstar kits from Ambion), and titer confirmed by SDS gel analysis of capsid protein VP3. AAV titers were 1 X 10^{13} virus/mL.

2.3. Transduction of mice with AAV and euthanasia

Expression of RLC-GFP was induced by the transduction of ~3-month-old mice via retro-orbital injection with 100 μl of AAV. Based on the measured half-life of the endogenous RLC [11]. the mice were allowed to replace RLC for 12 ± 2 days post-transduction. Mice were anesthetized with isoflurane and euthanized by cervical dislocation. Hearts were harvested for protein quantification, protein purification, and/or two-photon imaging. Photographs were taken for morphological comparison, and heart/body weight ratios (±SD) were determined for age- and sex-matched FVB wild type (N=3) and AAV-transduced (N=3) mice and compared using an unpair Student's t-test.

2.4. Quantification of the abundance of RLC-GFP

To quantify the abundance of the endogenous RLC and RLC-GFP expressed in the hearts of mice treated with the AAV, small 1-2 mg pieces of left ventricles from FVB wild type (N=4) and AAV-transduced (N=4) mice were digested with trypsin, and protein abundances were quantified by label-free liquid chromatography mass spectrometry (LCMS), as previously described [11]. Briefly, each piece of muscle was mechanically triturated with forceps in a glass bottom dissection chamber containing 150 μl 0.1% Rapigest SF Surfactant (Waters Corporation). The proteins were reduced by addition of 0.75 μl 1 M dithiothreitol (DTT), and heating at 100 °C for 10 min. The proteins were alkylated by adding 22.5 μl of a 100 mM iodoacetamide in 50 mM ammonium bicarbonate, and incubating for 30 minutes in the dark at ~22 °C. The proteins were cleaved into tryptic peptides by adding 25 μl of 0.2 μg/μl trypsin (Promega) in 50 mM ammonium bicarbonate, and incubating for 18 h at 37 °C. Following the digestion, the samples were dried down by centrifugal evaporation and reconstituted in 100 μl of a 7% formic acid in 50 mM ammonium bicarbonate solution to inactivate trypsin and degrade Rapigest (1 h, 37 °C). Samples were dried down once more and reconstituted in 100 μl 0.1% trifluoroacetic acid (TFA) for further cleavage of Rapigest (1 h, 37 °C). Samples were dried down a final time, reconstituted in 150 μl 0.1 TFA, centrifuged for 5 min at 18,800 RCF (Thermo, Sorvall Legend Micro 21R), and 125 μl of the supernatant was removed for analysis by mass spectrometry.

Tryptic peptides were separated via high-pressure liquid chromatography (LC) on an Xselect HSS T3 column (100 Å, 3.5 μm, 1 × 150 mm) (Waters Corporation) attached to an UltiMate 3000 ultra-high-pressure liquid chromatography system (Dionex). A 20-μL aliquot of each sample was injected into 0.1% formic acid in 2% acetonitrile with a flow rate of 100 μl/min. The LC parameters were identical to those previously reported [11]. The LC effluent was directly infused into a Q Exactive Hybrid Quadrupole-Orbitrap mass spectrometer (Thermo) through an electrospray ionization source. The instrument was operated in positive electrospray ionization mode using data dependent MS parameters identical to those previously reported [11]. Data were collected as Thermo Xcalibur .raw files.

To quantify the abundance of RLC relative to myosin heavy chain in each sample, peptides were identified, and LCMS peak areas were quantified from the .raw files using Thermo Proteome Discoverer 2.2.0.388 (PD 2.2). The .raw files were searched using Sequest HT against a Mus musculus database (containing 74,085 sequences, downloaded 02/09/15 from Uniprot). The database was digested *in silico* using trypsin, and up to two missed cleavages were permitted. The search parameters included carbamidomethyl as a variable modification of cysteine and variable modifications accounting for oxidation (Met, Pro), dioxidation (Met), and phosphorylation (Arg, Ser, Thr, Tyr).

The relative abundance of RLC to myosin heavy chain was determined from the average abundance of top 3 ionizing peptides from RLC divided by the average abundance top 3 peptides ionizing peptides shared between MYH6 and MYH7 in each sample. The average relative abundances ± SD were reported for each group. The fraction of the RLC that contained GFP fused to it C-terminus was determined by mass balance from the difference in the abundance of the C-terminal peptide resulting from the digestion of endogenous RLC in each sample. The average abundance ± SD were reported for the AAV-transduced mice.

2.5. Protein preparation for *in vitro* motility assays

Myosin molecules were purified from ~30 mg pieces of ventricular tissue from the apex of FVB wild type (N=3) and AAV-transduced (N=3) hearts, as previously described [20]. Briefly, mice were euthanized by cervical dislocation, the apex removed, and homogenized in extraction buffer (300 mM KCl, 150 mM K_2HPO_4, 10 mM $Na_4P_2O_7$, 1 mM $MgCl_2$, 2 mM DTT, 1 mM ATP, pH 6.8). Cell debris was pelleted at 65,000 RPM for 1 hr at 4 °C, and the supernatant was decanted. The supernatant was then diluted 5,000x in 2 mM DTT and incubated at 4 °C for ≥ 1 hr for myosin filament formation. Myosin filaments were pelleted at 25,000 RPM at 4 °C for 20 minutes, and solubilized in storage buffer (600 mM KCl, 20 mM Imidazole, 20 mM DTT, pH 6.8) for ≥ 1 hr. Skeletal actin was purified from chicken pectoralis muscle and labeled with equimolar tetramethyl-rhodamine-phalloidin (TRITC) as previously described [21].

2.6. *In vitro* motility assays

In vitro motility assays (IVM) were performed as previously described [20]. Briefly, myosin molecules isolated from the GFP-labeled or unlabeled wild type mouse hearts were diluted to 100 μg/ml in myosin buffer (300 mM KCl, 25 mM Imidazole, 4 mM MgCl2, 1 mM EGTA, 10 mM DTT) and added to a nitrocellulose-treated flow cell. Assays were performed in motility buffer (25 mM KCl, 25 mM Imidazole, 4 mM $MgCl_2$, 1 mM EGTA, 10 mM DTT, 1 mM ATP, 1 mM phosphocreatine, ~1 μM creatine phosphokinase, 0.5% methyl cellulose) at 30 °C. The velocities of TRITC-actin filaments were visualized by epifluorescence imaging on a custom-built Nikon-based microscope and 200 images were recorded at a rate of 10 frames/s. Average actin sliding velocities were determined from six movies from each preparation using Diatrack, an automated tracking program [22]. Both the mean velocity from the image series ± SD and the frequency distribution of all individual filaments were graphed using Prism 10. Data were compared using a Student's test.

2.7. *Ex vivo* heart preparation for two-photon imaging

AAV-transduced mice were euthanized (N=4), their left ventricle was splayed open and their whole heart was pinned to a Sylgard (Dow Corning) coated dish to expose the papillary muscle. The preparation was immediately covered in 10 mL of Tyrode's Solution (137 mM NaCl, 2.7 mM KCl, 1 mM $MgCl_2$, 0.2 mM Na_2HPO_4, 12 mM $NaHCO_3$, 5.5 mM glucose, 10 μM ATP, ~1 μM creatine phosphokinase, pH 7.4) for duration of the FRAP experiments.

2.8. Two-photon imaging and FRAP

Imaging was performed using a laser-scanning Zeiss LSM-7 multiphoton system with a 20x Plan Apo 1.0 NA DIC VIS-IR water immersion lens. The sample was excited using a Coherent Chameleon Vision II Titanium Sapphire pulsed IR laser set to 900 nm at an intensity of 8.0 ± 1% and gain of 800. An average scan speed of 0.056 s^{-1} was used to collect images with a 102.5 nm × 102.5 nm pixel size. For the FRAP experiments, the fluorophores were quenched within 16 random three-dimensional subcellular volumes, being 1-2 μm in depth, distributed between eight individual cells, from the four *ex vivo* heart preparations. The laser was set to 900 nm, with 26% intensity, and the regions scanned for 8-10 iterations. Recovery was detected by capturing an image every 30 seconds for 30 minutes. Z-stacks were collected in 1 μm-steps before and after imaging to ensure recovery was not an artifact due to drift in the Z-axis of the microscope focal plane.

2.9. Two-photon image analysis

Images were viewed and intensities for each pixel of interest (102.5 nm/pixel) were plotted using Fiji (Image J) [23]. FRAP was determined for 20 individual sarcomeres collected from 4 different heart preparations. The peak intensity was measured as the average intensity spanning ± 307.5 nm from the center of the peak. Fluorescence intensities were normalized to unbleached sarcomeres in each image to account for photobleaching in the overall field of view during the experiment. The normalized intensity for each frame within specific regions of interest (ROI) was determined using Equation 1:

$$I_{frap-norm(t)} = \frac{I_{frap(t)} - I_{frap-bleach}}{I_{frap-pre} - I_{frap-bleach}} \quad (1)$$

in which $I_{frap-norm(t)}$ is the normalized intensity of the ROI at time t, I_{frap} is the raw intensity of the ROI, $I_{frap-bleach}$ is the raw intensity of the ROI immediately after photobleaching, and $I_{frap\text{-}pre}$ is the raw intensity of the ROI prior to photobleaching. Where indicated, a 3-point moving average was used for smoothing. The average intensities ± SEM were plotted versus time and fitted with a single exponential regression using Prism 9.2.0. The rate constant, half-life, and plateau of recovery (± their respective 95% confidence intervals), and the coefficient of determination (R^2) were reported.

To determine whether the rate of RLC-GFP mobility varied along the length of the thick filaments, we determined the rate constant for the change in fluorescence intensity within single pixels (102.5 x 102.5 nm) along the longitudinal axis of 4 sarcomeres. These data ±

SD were fitted with a linear regression and an extra sum-of-squares F test was used to test whether the slope was significantly different than 0 using Prism 9.2.0.

2.10. Filament polymerization assays

Myosin was extracted from wild type FVB mouse hearts (N=3) as described for the *in vitro* motility assays. Myosin (~1 mg/ml) was stored in high salt buffer (600 mM KCl, 25 mM imidazole, 1 mM EGTA, 4 mM $MgCl_2$, 6.7 mM DDT, 0.7 mM ATP, 8 μg/ml phosphocreatine). Purified myosin was then diluted to 0.2 mg/ml in a mixture of high salt buffer and low salt buffer (25 mM KCl, 25 mM Imidazole, 1 mM EGTA, 4 mM $MgCl_2$, 6.7 mM DDT, 0.7 mM ATP, 8 μg/ml creatine phosphate,) to achieve desired concentrations of potassium chloride. The myosin was incubated overnight at 4 °C, to allow for filament formation.

Filaments were separated from soluble myosin by centrifugation at 13,700 RPM for 30 minutes at 4 °C and decanting of the supernatant. A 10-μl aliquot of 0.1 M BSA was then added to each supernatant and pelleted fraction for normalization. The samples were then dried down by centrifugal evaporation. Each sample was resuspended in 75 μl 50 mM ammonium bicarbonate with the addition of 5 μl 0.1 M DTT and heated for 10 minutes at 100°C. The samples were then treated with 10.4 μl of 0.1 M iodoacetamide for 30 minutes in the dark at room temperature. A 25-μl aliquot of a 0.2 μg/μl trypsin (Promega) in 50 mM ammonium bicarbonate solution was added to each sample and they were digested for 18 hours at 37 °C. Following digestion, a 100-μl aliquot of 7% formic acid in 50 mM ammonium bicarbonate was added to inactivate trypsin, and samples were dried down by centrifugal evaporation.

The samples were resuspended in 0.1% trifluoroacetic acid (TFA), centrifuged for 5 minutes at 18,800 RCF, and the supernatant was analyzed by liquid chromatography mass spectrometry (LCMS) as described in Section 2.4, and previously [11, 24]. The .raw files were searched using Sequest HT against a Mus musculus database (containing 74,085 sequences, downloaded 02/09/15 from Uniprot) including the sequence for bovine serum albumin, using Proteome Discoverer 2.2.0.388 (PD 2.2). The database was digested *in silico* using trypsin, and the search parameters were identical to those described in Section 2.4. The relative abundance of each protein of interest was obtained from the average abundance of the top 3 ionizing peptides divided by the average abundance of the top 3 ionizing peptides from BSA in each sample. The percentage of each protein in the soluble fraction was defined as the abundance of the protein in the soluble fraction divided by the summed abundance of the protein in both fractions. The relative abundance of RLC phosphorylation was measured between fractions from the abundances of the non-phosphorylated IEGGSSNVFSMFEQTQIQEFK peptide, containing serine 13 and 14, divided by the average abundance of the top 3 RLC peptides in each sample. Noting, this is not a quantitative measurement of the absolute abundance of RLC phosphorylation in these samples. Each experimental condition was carried out with a minimum of three replicates.

2.11. Microfluidic diffusional sizing (MDS)

Myosin was extracted from AAV-transduced hearts (N=3) as described for the *in vitro* motility assay. Myosin was solubilized in high salt tris buffer (400 mM KCl, 10 mM Tris, 1 mM DTT, pH 7.4), then diluted in low salt tris buffer (10 mM Tris, 1 mM DTT, pH 7.4) to achieve desired concentrations of potassium chloride, and incubated overnight at 4 °C. Samples were also prepared in the presence of 5 mM, 10 mM, or 20 mM ethylenediaminetetraacetic acid (EDTA) to determine the impact of calcium chelation on RLC.

Just prior to MDS measurements, samples were centrifuged at 13,700 RPM for 30 minutes at 4 °C. The supernatants were retained and the filament-containing pellets were discarded. A 3.5-4-μL aliquot of soluble myosin was loaded on a microfluidic chip (Fluidic Analytics, Cambridge, UK) for MDS analysis [25]. The MDS measurements were performed at room temperature on a Fluidity One-M Serum (Fluidic Analytics, Cambridge, UK) using a 488 nm LED with the size range set at 2-20 nm and a viscosity setting of 1. The MDS device uses a proprietary microfluidic chip with two channels: one channel, the sample channel, contains the fluorescently labeled myosin sample, while the other channel, auxiliary channel, contains tris buffer with matching potassium chloride concentration. Due to specific channel size and flow rates, low Reynolds numbers can be achieved as a result of laminar flow, allowing particles to move into the auxiliary stream by diffusion only. The rate of diffusion depends on the size of the species. At the end of the diffusion chamber, the streams are split and the fluorescence of both the diffused and undiffused material is measured. The ratio of fluorescence signals in the two channels is used to calculate the hydrodynamic size of the fluorescently labeled species. Thus, MDS provides the mass-average hydrodynamic size of the labeled species in the sample using the Stokes-Einstein Equation:

$$D = \frac{k_B \cdot T}{6 \cdot \pi \cdot \eta \cdot r_H} \tag{2}$$

in which D is the diffusion coefficient, k_B is Boltzmann's constant, T is the temperature, η is the viscosity of the solution, and r_H is the hydrodynamic radius. The average Stokes radii measured across concentrations of potassium chloride were then fit to the Arrhenius equation (Eq. 3) using linear extrapolation to determine free energy of unfolding and the fraction folded at each salt concentration:

$$K_{eq} = e^{-\Delta G + mx / RT} \tag{3}$$

in which K_{eq} is the equilibrium constant, ΔG is the free energy of unfolding (in kcal/mol), m is the slope of the curve at the transition between the folded and unfolded state, x is the molarity of potassium chloride, R is the ideal gas constant (0.199 kcal·K^{-1}·mol^{-1}), and T is

the temperature (in K). Differences in hydrodynamic radii under different conditions were determined using an unpaired Student's T-test.

3. Results

3.1. GFP-labeled RLC (RLC-GFP) replaces a fraction of endogenous RLC and has no effect on actin sliding.

To examine the mechanism(s) by which individual molecules exchange into and out of thick filaments within sarcomeres in intact hearts, we labeled myosin regulatory light chain (RLC) with a fluorescent tag. An adeno-associated virus (AAV) was designed using the TnT promoter to express cardiac myosin regulatory light chain (RLC) with a green fluorescent protein (GFP) fused to its C-terminus. Adult mice (~3 months of age) were transduced with the AAV, and the mice were allowed 12 ± 2 days to replace the endogenous RLC by protein synthesis and degradation. Neither the morphology (Fig. S1A) nor the heart/body mass ratio for the AAV transduced hearts (4.35 ± 0.25 mg/g) differed ($p=0.40$) when compared to age- and sex-matched wild type FVB hearts (4.76 ± 0.70 mg/g). The abundance, function, and localization of the RLC-GFP within the AAV transduced hearts were quantified using multiple approaches.

To quantify the abundance of the RLC-GFP expressed, small 1-2 mg pieces of left ventricles were digested with trypsin, and protein abundances were quantified by label-free liquid chromatography mass spectrometry (LCMS). The average abundance of the top 3 ionizing peptides resulting from the digestion of RLC was determined relative to those from the digestion of myosin heavy chain. These apparent relative abundances of RLC did not differ between the four AAV transduced and four wild type control mice (0.73 ± 0.07 to 1 myosin heavy chain, versus 0.72 ± 0.04 to 1 myosin heavy chain, respectively). However, 22 ± 7% (SD) of the endogenous RLC was replaced with RLC-GFP in the transduced mice, as measured from the difference in the abundance of the C-terminal peptide, generated from the digestion of the endogenous RLC in each sample. These data demonstrate that RLC-GFP replaced a significant fraction of the endogenous RLC while retaining the native stoichiometry of RLC observed in wild type mice.

Next, we tested whether having GFP fused to the C-terminus of RLC impacted actin filament sliding using an *in vitro* motility assay. Myosin molecules were isolated from ~30 mg pieces of the left ventricle of three AAV-transduced and three wild type mouse hearts. In each experiment, myosin was deposited onto the surface of a flow-cell, and the average velocity of tetramethyl-rhodamine-labeled actin filaments sliding over these molecules was determined using epifluorescence microscopy (1 mM ATP, 30 ° C). Neither the sliding velocity (Figs. 1C, S1B) nor the fraction of actin filaments moving (86 ± 6 vs. 89 ± 5%) differed on the myosin isolated from the AAV-transduced or wild type mouse hearts ($P=0.987$ and $P=0.667$, respectively). These data demonstrate that the GFP-tag had no effect on actin filament sliding, as measured in the *in vitro* motility assay.

3.2 RLC-GFP is localized to the heads of myosin molecules within thick filaments.

To determine whether the RLC-GFP was properly localized within the heart, the papillary muscle of *ex vivo* heart preparations was imaged using two-photon confocal microscopy (Fig. 1D inset). At low magnification (1,190 nm / pixel), GFP labeling was visible within the boundaries of cardiomyocytes deep within the papillary muscle (Fig. 1D, Movie S1). Dark regions were present in these images that corresponded to structural features such as nuclei and intercalated disks (Fig. 1D). At high magnification (102.5-nm pixel size), dark striations were visible along the longitudinal length of cells (Figs. S1A) or as shown along the x-axis of Fig 2A. This spacing was consistent with the localization of Z-discs between neighboring sarcomeres in relaxed cardiac muscle cells [26].

To further define the distribution of the RLC-GFP within single sarcomeres, the bands in fluorescence intensity along the longitudinal axis of multiple myofibrils were averaged (Fig. 2B). The average fluorescence plot profile was characterized by a peak with two subtle maxima (Fig. 2B – dashed line). The width of this peak at half-maximal intensity was ~1.6-μm, being similar in length to the length of native, striated muscle thick filaments (1.65 μm, [27]). The small dip in fluorescence in the center of the peak (Fig. 2B – arrow) was indicative of the 170 nm bare zone of the thick filament [27], which is devoid of myosin heads (Fig. 1A). These features indicate that RLC-GFP is properly incorporated into the thick filaments within the sarcomere.

Previous studies using electron or super-resolution fluorescence microscopy demonstrate that myofibrils run in parallel along the axial length of the cells [28, 29]. Therefore, with sufficient resolution there should be gaps in the fluorescence intensity along the y-axis of the striations in Fig 2A. Yet these gaps were not always readily visible by eye, even in these high magnification images. To define the orientation of adjacent myofibrils, average fluorescence intensity profiles were generated along the y-axis of the striations (Fig. 2D). Minima were observed in fluorescence intensity profile every 1-2 μm (Fig. 2E) due to the physical separation of the myofibrils. To confirm the physical separation between myofibrils (Fig. 2F), two-photon images were collected near the edges of the heart preparation, where cells were arranged axially to the imaging plane (Fig. S1B). Puncta of fluorescence, being 1-2 μm in diameter, were observed in these cross-sectional images. These dimensions were consistent with the width of myofibrils in cardiac muscle cells [28, 29]. Together, the fluorescence profiles collectively demonstrate that the RLC-GFP is highly localized A-bands within relaxed sarcomeres, located within myofibrils arranged in parallel.

3.3. Fluorescence recovery was not observed after photobleaching whole sarcomeres.

To determine whether the localization of the RLC-GFP is static or dynamic in the cardiac muscle cells, the fluorophores within 16 random three-dimensional subcellular volumes, being 1-2 μm in depth, were irreversibly photobleached with a high-intensity laser, and fluorescence recovery after photobleaching (FRAP) was monitored for 30 minutes with two-photon confocal imaging (Figs. 3–4, Movies S2–S3). Average fluorescence intensity profiles were generated for regions of interest (ROI) along the x- and y-axes of these images. These profiles were first used to define the localization and orientation of individual

sarcomeres within the images, as demonstrated in Fig. 2. The profiles were then used to define the portion of the cell that had been photobleached.

Within two of the 16 photobleached regions, the volume appeared to capture the entire contents of the sarcomere. An example of this is demonstrated in Fig. 3A–E and illustrated in Fig. 3F. The fluorescence intensity profiles generated from this region of the cell suggest it contains five myofibrils organized in parallel (labeled I-V in Fig. 3D), that each contains three sarcomeres (labeled 1-3 in Fig. 3E). Photobleaching (Fig. 3B) resulted in the loss of fluorescence from all the RLC-GFP molecules within four sperate sarcomeres (sarcomeres 2 and 3 in myofibrils II and III). This loss is demonstrated by the red lines in Fig. 3D–E. Under these conditions, no FRAP occurred in any of these sarcomeres within 30 minutes after photobleaching, as demonstrated by the grey lines in Fig 3D–E).

Importantly, when a bleached sarcomere (sarcomere 2) was adjacent to an unbleached sarcomere (sarcomere 1) within a myofibril (myofibrils II and III), the RLC-GFP did not move from the unbleached sarcomere into the bleached sarcomere within 30 minutes. Similarly, when a bleached sarcomere (sarcomere 2) was adjacent to an unbleached sarcomere (sarcomere 2) in parallel myofibrils (myofibrils II and I), the RLC-GFP did not move from the unbleached sarcomere into the bleached sarcomere within 30 minutes. The lack of FRAP when the entire volume of the sarcomere was photobleached demonstrated that: (a) the RLC-GFP is irreversibly photobleached, (b) myosin does not exchange between sarcomeres separated by Z-discs, (c) myosin does not exchange between neighboring myofibrils, being separated by sarcoplasmic reticulum and mitochondria, and (d) the synthesis of new RLC-GFP molecules is not detected in the *ex vivo* heart preparations.

3.4. RLC-GFP was highly mobile within the confines of a single sarcomere.

To determine whether the localization of the RLC-GFP is static or dynamic within the boundaries of a single sarcomere, FRAP was quantified in the three-dimensional volumes in which only a portion of a sarcomere was irreversibly photobleached. An example of this is demonstrated in Fig. 4 and Movie S3. The photobleached region in Fig. 4B–C marked with a yellow asterisk is analogous to the region shown in Fig. 3, in which the vast majority of the RLC-GFP within each sarcomere is photobleached and there is no FRAP within 30 minutes. In contrast, the photobleached region marked with the red asterisk in Fig. 4B demonstrated rapid FRAP. This region contained two myofibrils arranged in parallel, that each contained three sarcomeres. These six sarcomeres were partially photobleached along their longitudinal axis.

The region of interest (ROI) highlighted in these images (Fig 3A–D), was selected for quantification of FRAP (Fig. 3E). This ROI contained two sarcomeres, from the neighboring myofibrils, and a portion of the RLC-GFP within each sarcomere was photobleached along their longitudinal axes. Within the photobleached portion of these sarcomeres, FRAP was observed within minutes and the fluorescence intensity in the non-bleached portion of the same sarcomere decreased (Fig. 4D–E). These data demonstrate that the localization of the RLC-GFP molecules was highly mobile within the confines of the sarcomere, as illustrated in Fig. 4F.

To determine the rate of RLC-GFP mobility within single sarcomeres and the fraction of molecules that were mobile, FRAP was quantified from 20 partially bleached sarcomeres from four different *ex vivo* whole heart preparations (Figs. 4G, S2). The average relative intensities were plotted versus time, and the data were fitted with a single exponential equation (Fig. 4G). This curve yielded a rate constant of 0.14 (± 0.13 to 0.16) min^{-1}, half-life of 4.8 (± 4.3 to 5.5) minutes, and plateau of 0.70 (± 0.67 to 0.73) with R^2 being 0.996. These data demonstrate the RLC-GFP is highly mobile within the confines of a single sarcomere, with FRAP occurring from the exchange of molecules in thick filaments from one region of the sarcomere, with those from another region of the same sarcomere.

3.5. RLC-GFP motility may be greater at the tips of the thick filaments.

To determine whether the rate of RLC-GFP mobility varied along the length of the thick filaments, we quantified the change in fluorescence intensity in single pixels (102.5 x 102.5 nm) along the longitudinal axis of 4 sarcomeres (Fig. 5A). Nearest to the center of the sarcomere, the rate constant of recovery was 0.23 ± 0.09 min^{-1}. Within the C-zone (180-530 nm from the M-line), where the thick filament contains myosin, MyBP-C, and titin, the rate constants were nearly identical to those near the M-line. Nearest the tips of the thick filaments, where the myosin heads are less densely packed [30], the rate constants appeared to increase up to 0.37 ± 0.11 min^{-1}. If the rate constants were independent of position along the length of the thick filament these data should be well-fitted by a linear regression with a slope equal to 0. However, these data were not well fitted with a linear regression (R^2=0.50) and the slope of the fit was significantly (P=0.033) greater than 0 (Fig. 5A, dashed line). These data collectively demonstrate that exchange occurs along the entire length of the thick filament but there may be an increase in the rate of exchange toward the tip of the thick filaments.

3.6. RLC-GFP remained tightly bound to myosin heavy chain which adopted a folded and/or compact confirmation when disassociated from the thick filament.

To determine whether the stoichiometry of RLC and myosin heavy chain is conserved when disassociated from the thick filaments, thick filament proteins were purified from ~30 mg pieces of wild type heart ventricles (N=4), depolymerized with high ionic conditions, and then repolymerized by lowering the ionic conditions (4 °C). These processes resulted in the generation of ionic strength-dependent filamentous and soluble fractions of thick filament proteins. The relative abundance of RLC, ELC, and myosin heavy chain were identical within the soluble and filamentous fractions under all conditions (Fig. S3A). These data suggest RLC, ELC, and myosin heavy chain remains tightly bound together, presumably as single myosin molecules, when dissociated from the thick filaments. Under the experimental conditions tested, 100% of the molecules remained soluble at high ionic conditions (>250 mM KCl), and only 20% of them were soluble at 150 mM KCl (Fig. 5B).

The LCMS analyses identified peptides containing both single and dual phosphorylation of serine 13 and 14 on the RLC in both the soluble and filamentous fractions. To determine whether the level of phosphorylation affected RLC solubility, the abundance of non-phosphorylated RLC peptide was determined relative to the average abundance of the top 3 RLC peptides in each sample (Fig. S3B). The non-phosphorylated peptides were

distributed equally between the fractions (Fig. S3B), which demonstrates that the formation of thick filaments in not dependent on RLC phosphorylation, under these experimental conditions.

To further define whether the RLC-GFP remained bound to the heavy chain in the soluble fraction, we repeated these experiments with thick filament proteins isolated from the GFP-transduced heart ventricles (N=4), and determined the Stokes radius of the RLC-GFP in the soluble fraction using microfluidic diffusional sizing (MDS). If the RLC-GFP was dissociated from the myosin heavy chain, the Stokes radius was predicted to be ~3.1 nm [31]. However, the Stokes radii ranged from 12.0 ± 0.9 nm at the lowest ionic conditions, to 18.2 ± 0.8 nm at the highest concentration of KCl (Fig. 5C). These data demonstrate that the Stokes radii were much larger than that predicted for RLC-GFP and they were dependent on ionic conditions.

To determine whether the large Stokes radii were an artifact of the MDS assay, the experiments were repeated with the addition of 5-20 mM ethylenediaminetetraacetic acid (EDTA), a divalent ion chelator which allows for the release of the RLC-GFP from the myosin heavy chain [32]. Under these conditions, there was a significant drop ($p < 0.01$) in the Stokes radii in the presence of EDTA at each of the ionic conditions examined (Fig. 5D), when compared to the radii in the absence of EDTA. Interestingly, the radii measured by MDS in the presence of EDTA (6.4-10.7 nm) were also significantly larger than the ~3.1 nm radius predicted for the RLC. These data imply that only a fraction of the RLC-GFP remained disassociated from the myosin molecules in the presence of EDTA, under these experimental conditions.

4. Discussion

We recently demonstrated that the half-life of the thick filament proteins in adult mouse heart ventricles is ~10 days and the mechanism involves the stochastic replacement of individual molecules rather than intact thick filaments [11]. These data support a seminal hypothesis by Dr. Brenda Russell/Eisenberg suggesting that myosin molecules are translated at the boundaries of sarcomeres, and randomly inserted into thick filaments [33]. In order to define the spatial and temporal aspects of this replacement, we sought to label newly synthesized myosin molecules with a fluorophore and visualize their localization within thick filaments in intact cardiac muscle using two-photon microscopy. We designed an adeno-associated virus (AVV) to express myosin regulatory light chain (RLC) with green fluorescent protein (GFP) fused to its C-terminus, as labeled myosin heavy chain was too large to fit in an AAV vector. Transduction of adult mice resulted in the partial replacement of the endogenous RLC with the RLC-GFP that was properly localized to the head region of myosin heavy chain and did not affect the ability of myosin to translocate actin filaments *in vitro*.

Having GFP fused to RLC within the thick filaments enabled us to quantify the extent of the mobility of the RLC within *ex vivo* heart preparations using fluorescence recovery after photobleaching (FRAP). In the experiments, multiple areas within single cells deep within the papillary muscle were photobleached and FRAP was analyzed. The RLC-GFP mobility

was dependent on the size of the photobleached area, with no mobility being observed when all the RLC-GFP molecules within a sarcomere were photobleached (Fig. 3, and region noted with yellow asterisk in Fig. 4). When coupled with our previous report which defined the half-life of RLC in mice of similar age being ~10 days [11], the lack of recovery demonstrated that RLC-GFP could not diffuse through the Z-discs discs of neighboring sarcomeres, or between myofibrils located in parallel. This observation seems reasonable considering the Z-discs flanking the ends of each sarcomere, and sarcoplasmic reticulum and/or mitochondria separating myofibrils, would present significant physical barriers for diffusion. However, it is possible that such mobility may occur over a longer timescale or between immature sarcomeres in cellular assays.

Other groups have applied FRAP to quantify the mobility of myosin heavy chain, or other sarcomeric proteins such as titin, in skeletal and/or cardiac muscle cells *in vitro*. In these reports, large regions of the cells were photobleached which encompassed many sarcomeres within many myofibrils. FRAP appeared to occur homogenously within these regions in hours, suggesting that the localization of these proteins was also mobile [34–38]. Interestingly, these studies did not report the rate of protein synthesis in their model systems. Therefore, it is unclear if FRAP resulted from the replacement of photobleached molecules with newly synthesized molecules or from the movement of these molecules through these physical boundaries on a longer timescale. Regardless of the mechanism, all these studies suggest the structure of the sarcomere is highly dynamic.

In contrast to these earlier studies, we focused most of our analyses on single sarcomeres in which only a fraction of the RLC-GFP molecules had been photobleached. An example of this scenario was demonstrated in the photobleached region of Fig. 4B–C that was marked with a red asterisk. This region contained two myofibrils running in parallel, in which a portion of each myofibril was photobleached along their longitudinal axes. The region of interest (ROI) in Fig. 4A–D contained two sarcomeres organized within these neighboring myofibrils. The fluorescence intensity in the photobleached portion of each sarcomere increased as the fluorescence intensity in the unbleached portion of the sarcomeres decreased (Fig. 4D–E). This phenomenon was contrasted to that observed in the lower photobleached region of Fig 4B–C marked with a yellow asterisk, which demonstrated no FRAP. The presence of these two distinctively different photobleached regions within the same image series demonstrated the FRAP is not an artifact due to drift in the Z-axis of the microscope focal plane.

The vast majority of the RLC-GFP was bound into the A-band of the sarcomere (Fig. 2B). Therefore, we interpreted the reciprocal changes in the fluorescence intensity in partially bleached sarcomeres to result from the release of molecules from the thick filament into a cytoplasmic pool of monomers, diffusion of these molecules in the space between filaments, and reincorporation of the molecule into a new site (illustrated in Fig. 4F). This observation is consistent with pioneering work by Josephs and Harrington that suggested an equilibrium exists between filamentous and soluble myosin [14].

To further define the temporal aspects of FRAP, the analyses were expanded to several partially bleached sarcomeres (N=20) in multiple *ex vivo* heart preparations (N=4). The

RLC-GFP FRAP was well fitted by a single exponential (R^2=0.996) and reached a plateau within minutes (Fig. 4G). The half-life of this process ($t_{1/2}$=4.8 min) is similar to that reported for the exchange of myosin molecules between synthetic thick filaments *in vitro*, where 50% of the molecules were exchanged in <10 min [17], but faster than that previously reported for myosin heavy chain in cellular assays [34–36]. The plateau of the average exponential was 70 (67 to 73%) of the initial intensity (Fig. 4G). Our assay did not have the spatial resolution to quantify the exact volume of each sarcomere photobleached, but if we assume ~30% of the RLC-GFP molecules in each sarcomere were photobleached and 100% of the molecules are mobile, then 70% of the initial fluorescence intensity would remain. Such mobility is supported by the reciprocal relationship between the change in position of the photobleached and fluorescent RLC-GFP (Fig. 4D–E).

While all of the RLC-GFP in the thick filaments appeared mobile, the rate of mobility was not homogenous along the length of the sarcomere (Fig. 5A). At the center of the sarcomere, the tails of myosin heavy chain are packed in an antiparallel arrangement and interact with M-line proteins [39]. In the C-zones, the tails of myosin heavy chain interact with both MyBP-C and titin [40, 41]. Despite these differences, similar rates of recovery were observed in these regions (Fig. 5A). In contrast, there appeared to be an increase in the rate of recovery within the tips of the filaments, located closest to the Z-discs of the sarcomere (Fig. 5A). This trend suggests that either the RLC-GFP or intact myosin may more readily exchange into and out of the tips of the filaments where the myosin molecules are less densely packed [30]. These data were supported by our previous report in which we demonstrated that myosin molecules initially depolymerize from the tips of the filaments when the cells are skinned and exposed to ionic solutions [11]. This was also supported by Ichimura et al., which demonstrated faster exchange of myosin heavy chain at the tips of filaments in intact skeletal muscle cells [42]. Taken together, these data imply the structural arrangement of the RLC-GFP at the tips of the cardiac thick filament may be the most dynamic.

The fluorescent label in the FRAP experiments was fused to the RLC, and therefore the mobility could have been due to the exchange of RLC molecules between myosin heavy chains or the exchange of whole myosin molecules between filaments. The FRAP data were well-fitted (R^2=0.996) by a single exponential and therefore are likely the result of a single process. To distinguish between mechanisms, we isolated myosin molecules and took advantage of the established ionic strength-dependence of myosin filament formation [43] to determine whether the stoichiometry of RLC to myosin heavy chain was similar between thick filaments and soluble molecules. At the lowest ionic conditions (150 mM KCl), approximately 20% of the RLC, essential light chain, and myosin heavy chain were found in the soluble fraction. This was similar to that observed for skeletal muscle myosin observed *in vitro* polymerization assays [17]. Most importantly, the abundances of RLC, essential light chain, and heavy chain were equimolar in each fraction (Fig. S3A). These data suggested that the light chains were likely bound to the soluble heavy chains.

To confirm whether the conserved ratio of RLC to myosin heavy chain in the soluble fraction was indicative of the RLC being bound to the heavy chain, the Stokes radius of the RLC-GFP was measured using microfluidic diffusional sizing (MDS). Noting, MDS

relies on fluorescence detection to determine the radius of the labeled protein. The radius of the RLC-GFP was ionic strength dependent (Fig. 5C) but being much larger than the 3.1 nm radius predicted for RLC-GFP under all experimental conditions [31]. At the lowest ionic strength tested (150 mM KCl, Fig. 5C), only 20% of the myosin was soluble (Fig. 5B) and the Stokes radius (12.0 ± 0.9 nm) of the soluble myosin was similar to the 12.5 nm determined for folded (10S) smooth muscle myosin molecules [44, 45]. At higher ionic conditions (600 mM KCl), where nearly all the myosin was soluble (Fig 5A), the Stokes radius (18.2 ± 0.8 nm) was similar to the 18.5 nm radius of extended (6S) smooth muscle myosin [44, 45]. These radii suggested that the RLC-GFP were likely bound to intact myosin molecules.

The radii measured across ionic conditions were fitted with a sigmoidal curve using a derivation of the Arrhenius equation to predict the distribution of myosin molecules in the folded (Fig. 5C, inset) versus extended confirmation, and the free energy associated with unfolding. Half of the myosin was predicted to be in the folded conformation at 327 mM KCl, and > 90% of molecules folded at ≤ 200 mM KCl. The free energy of unfolding was determined to be 3.4 kcal/mol. This is approximately half of the energy required to disrupt the beta sheet interactions required to unfold a stable Ig domain, like the I27 domain of titin [46, 47] and was comparable to the energy required to unfold a weaker Ig domain, like A164 or I83 [47–49]. These data suggest that the compact structure is very stable at physiological ionic strengths without competing interactions.

The radii of the RLC-GFP only appeared smaller, when the soluble myosin was incubated with EDTA to weaken the binding between the RLC and myosin heavy chain [32]. Even under these non-physiological experimental conditions the range of values (6.4-10.7 nm) was significantly larger than the 3.1 nm radius predicted for RLC-GFP. These data suggest that a mixture of RLC bound to myosin heavy chain and free RLC exists in the presence of EDTA.

In the absence of EDTA at more physiological ionic conditions, the 12.5 nm radius suggested cardiac muscle myosin molecules adopt a similar conformation to 10S smooth muscle myosin. This conformation is stabilized by intramolecular interactions between segments of the coiled-coil tail to keep it in an inactive state [50, 51]. It has long-been established that phosphorylation of the smooth muscle RLC disrupts this folded state and promotes the extended, 6S conformation [44, 45, 52]. However, the structural transition between the folded and extended state for cardiac muscle myosin does not appear driven by the phosphorylation of the RLC because phosphorylated RLC was distributed equally between the soluble and filamentous fractions (Fig. S3B). Therefore, the folded configuration of cardiac myosin may be a thermodynamically driven process due, in part, to electrostatic interactions between segments in the highly charged tail. Structural studies of thick filaments and sarcomeres demonstrate that specific intermolecular interactions between regions of the tail are essential for the formation of the thick filament backbone [10, 40, 41]. It is likely that similar interactions occur between these regions within the same tail, to stabilize the folded conformation of cardiac muscle myosin.

While our findings suggest that soluble cardiac myosin adopts a folded, presumably inactive state while in the cytosol, many questions remain if folding could drive the exchange of myosin molecules into and out of thick filaments or if the RLC exchanges on the timescale of the FRAP experiments. In support of the former, smooth muscle cells contain a significant population of soluble myosin in the folded, 10S conformation [53]. While phosphorylation and extension of the myosin monomers is typically associated with filament formation [44, 45, 52], molecules in the folded, 10S configuration can assemble into filaments *in vitro* [45, 53]. This relationship between myosin folding and filament formation appears to be highly dynamic in smooth muscle cells and the rate of exchange *in vitro* is even faster than that observed in our experiments [54]. Therefore, it is possible that myosin filaments share this mechanism of exchange in striated [34–36], smooth [54], and even non-muscle systems [55].

Questions remain about whether the FRAP in the intact hearts resulted from the exchange of myosin molecules between thick filaments and/or exchange of RLC between heavy chains. Regardless, the results provide the first demonstration that the structure of the thick filament is highly dynamic in *ex vivo* heart preparations and the mobility of the components is restricted to the boundaries of the sarcomere. Surprisingly, the rate of exchange was ~1,500 times faster than that required to replace the RLC or myosin heavy chain through protein synthesis and degradation [11]. Interestingly, the molecular machinery required for protein replacement are localized at the periphery of the sarcomere [18, 19]. Therefore, this rapid exchange may be an intrinsic design feature of the sarcomere that allows for the continual movement of parts and pieces, allowing for “on-site” protein replacement while supporting contractile function [2]. Future studies will be targeted at understanding how this rate of exchange ultimately affects the generation of contractile force and motion and/or the rate of replacement of these proteins. It is possible that disease related mutations in contractile proteins such as myosin or myosin-binding protein C, and/or drugs targeted at perturbing myofilament mechanics affect these processes.

Limitations

While the use of two-photon microscopy to image intact *ex vivo* heart preparations brings us a step closer to visualizing the mobility of proteins within a single sarcomere *in vivo*, the hearts are non-contractile in our current manuscript. However, we do not have the technical expertise to stabilize the whole heart enough to keep the sarcomeres of interest in focus, while the heart is beating. It is possible that contractility may enhance or perturb intracellular mobility.

Secondarily, although our data demonstrate that the structure of the thick filament is dynamic, our label was fused to the regulatory light chain located on the myosin head. Although we have used *in vitro* assays to provide evidence that suggests the RLC-GFP remain tightly bound to the heavy chain, we cannot fully negate that FRAP may result from the RLC exchanging off and onto the myosin heavy chain. In the MDS experiments, the myosin molecules diffuse through a microfluidic chamber for 5 seconds, being shorter than the timescale of the observations in the FRAP assay. Albeit, if the RLC were exchanging between the heavy chains on a slower timescale, the MDS assay would not detect this

exchange. Future studies are aimed at using a CRISPER based approach to directly GFP-label the heavy chain in mouse *in vivo*.

Supplementary Material

Refer to Web version on PubMed Central for supplementary material.

Acknowledgements

Research reported in this project/publication was supported by the National Institutes of Health (NIH). Funds from the Heart, Lung, and Blood Institute (NHLBI) R01-HL157487 supported MJP, CMK, and Neil Wood, and Public Health Services T32-HL076122 supported CMK. Funds from the National Institute of General Medical Sciences (NIGMS) award number P20-GM135007, Core C: Customized Physiology and Imaging Core, supported the use of the Zeiss LSM 7. We thank Neil Wood for assistance with initial LCMS experiments, Dr. David Warshaw for use of epifluorescence microscope, Samantha Previs for preparation of actin used in assays, and Dr. Thomas Longden for the initial assistance and Todd Clason for continued assistance with the two-photon imaging.

References

[1]. Bergmann O, et al. Dynamics of Cell Generation and Turnover in the Human Heart. Cell 2015; 161(7): 1566–75. [PubMed: 26073943]

[2]. Martin TG, Kirk JA. Under construction: The dynamic assembly, maintenance, and degradation of the cardiac sarcomere. J Mol Cell Cardiol 2020; 148: 89–102. [PubMed: 32920010]

[3]. Willis MS, Schisler JC, Portbury AL, Patterson C. Build it up-Tear it down: protein quality control in the cardiac sarcomere. Cardiovasc Res 2009; 81(3): 439–48. [PubMed: 18974044]

[4]. Murakami U, Uchida K. Contents of Myofibrillar Proteins in Cardiac, Skeletal, and Smooth Muscles. The Journal of Biochemistry 1985; 98(1): 187–197. [PubMed: 4044549]

[5]. Hayashida M, Maita T, Matsuda G. The Primary Structure of Skeletal Muscle Myosin Heavy Chain: I. Sequence of the Amino-Terminal 23 kDa Fragment. The Journal of Biochemistry 1991; 110(1): 54–59. [PubMed: 1939027]

[6]. Lowey S, Cohen C. Studies on the structure of myosin. Journal of Molecular Biology 1962; 4(4): 293–IN17. [PubMed: 14466961]

[7]. Bennett PM. The structure of spindle-shaped paracrystals of light meromyosin. Journal of Molecular Biology 1981; 146(2): 201–221. [PubMed: 7021858]

[8]. Huxley HE. Electron microscope studies on the structure of natural and synthetic protein filaments from striated muscle. Journal of Molecular Biology 1963; 7(3): 281–308. [PubMed: 14064165]

[9]. Lowey S, Slayter HS, Weeds AG, Baker H. Substructure of the myosin molecule: I. Subfragments of myosin by enzymic degradation. Journal of Molecular Biology 1969; 42(1): 1–29. [PubMed: 4241282]

[10]. Sohn RL, Vikstrom KL, Strauss M, Cohen C, Szent-Gyorgyi AG, Leinwand LA. A 29 residue region of the sarcomeric myosin rod is necessary for filament formation. J Mol Biol 1997; 266(2): 317–30. [PubMed: 9047366]

[11]. Wood NB, Kelly CM, O'Leary TS, Martin JL, Previs MJ. Cardiac Myosin Filaments are Maintained by Stochastic Protein Replacement. Mol Cell Proteomics 2022; 21(10): 100274. [PubMed: 35921914]

[12]. Al-Khayat HA, Kensler RW, Squire JM, Marston SB, Morris EP. Atomic model of the human cardiac muscle myosin filament. Proc Natl Acad Sci U S A 2013; 110(1): 318–23. [PubMed: 23251030]

[13]. Zoghbi ME, Woodhead JL, Moss RL, Craig R. Three-dimensional structure of vertebrate cardiac muscle myosin filaments. Proc Natl Acad Sci U S A 2008; 105(7): 2386–90. [PubMed: 18252826]

[14]. Josephs R, Harrington WF. Studies on the formation and physical chemical properties of synthetic myosin filaments. Biochemistry 1966; 5(11): 3474–87. [PubMed: 5972328]

[15]. Katoh T, Konishi K, Yazawa M. Skeletal muscle myosin monomer in equilibrium with filaments forms a folded conformation. J Biol Chem 1998; 273(19): 11436–9. [PubMed: 9565554]

[16]. Saad AD, Dennis JE, Tan IP, Fischman DA. Visualization of myosin exchange between synthetic thick filaments. J Muscle Res Cell Motil 1991; 12(3): 225–34. [PubMed: 1874964]

[17]. Saad AD, Pardee JD, Fischman DA. Dynamic exchange of myosin molecules between thick filaments. Proc Natl Acad Sci U S A 1986; 83(24): 9483–7. [PubMed: 3467317]

[18]. Lewis YE, Moskovitz A, Mutlak M, Heineke J, Caspi LH, Kehat I. Localization of transcripts, translation, and degradation for spatiotemporal sarcomere maintenance. J Mol Cell Cardiol 2018; 116: 16–28. [PubMed: 29371135]

[19]. Aston D, et al. High resolution structural evidence suggests the Sarcoplasmic Reticulum forms microdomains with Acidic Stores (lysosomes) in the heart. Sci Rep 2017; 7: 40620. [PubMed: 28094777]

[20]. Previs MJ, Beck Previs S, Gulick J, Robbins J, Warshaw DM. Molecular mechanics of cardiac myosin-binding protein C in native thick filaments. Science 2012; 337(6099): 1215–8. [PubMed: 22923435]

[21]. Kron SJ, Spudich JA. Fluorescent actin filaments move on myosin fixed to a glass surface. Proc Natl Acad Sci U S A 1986; 83(17): 6272–6. [PubMed: 3462694]

[22]. Vallotton P, Olivier S. Tri-track: Free Software for Large-Scale Particle Tracking. Microscopy and Microanalysis 2013; 19(2): 451–460. [PubMed: 23448973]

[23]. Schindelin J, et al. Fiji: an open-source platform for biological-image analysis. Nature Methods 2012; 9(7): 676–682. [PubMed: 22743772]

[24]. O'Leary TS, Snyder J, Sadayappan S, Day SM, Previs MJ. MYBPC3 truncation mutations enhance actomyosin contractile mechanics in human hypertrophic cardiomyopathy. J Mol Cell Cardiol 2019; 127: 165–173. [PubMed: 30550750]

[25]. Fiedler S, et al. Antibody affinity governs the inhibition of SARS-CoV-2 Spike/ACE2 binding in patient serum. ACS Infect Dis 2021; 7(8): 2362–2369. [PubMed: 33876632]

[26]. van der Velden J, et al. Force production in mechanically isolated cardiac myocytes from human ventricular muscle tissue. Cardiovascular Research 1998; 38(2): 414–423. [PubMed: 9709402]

[27]. Squire JM. The Structural Basis of Muscular Contraction. 1981; Plenum Press, New York.

[28]. Previs MJ, et al. Myosin-binding protein C corrects an intrinsic inhomogeneity in cardiac excitation-contraction coupling. Sci Adv 2015; 1(1): e1400205. [PubMed: 25839057]

[29]. Rahmanseresht S, et al. The N terminus of myosin-binding protein C extends toward actin filaments in intact cardiac muscle. J Gen Physiol 2021; 153(3): e202012726. [PubMed: 33528507]

[30]. Craig R, Offer G. The location of C-protein in rabbit skeletal muscle. Proc R Soc Lond B Biol Sci 1976; 192(1109): 451–61. [PubMed: 4802]

[31]. Fleming PJ, Fleming KJ. HullRad: Biophysical Journal 2018; 114(4): 856–869. [PubMed: 29490246]

[32]. Chantler PD, Szent-Györgyi AG. Regulatory light-chains and scallop myosin: Full dissociation, reversibility and co-operative effects. Journal of Molecular Biology 1980; 138(3): 473–492. [PubMed: 6251228]

[33]. Russell B, Wenderoth MP, Goldspink PH. Remodeling of myofibrils: subcellular distribution of myosin heavy chain mRNA and protein. Am J Physiol 1992; 262(3 Pt 2): R339–45. [PubMed: 1558205]

[34]. Ojima K, et al. Myosin substitution rate is affected by the amount of cytosolic myosin in cultured muscle cells. Anim Sci J 2017; 88(11): 1788–1793. [PubMed: 28631391]

[35]. Ojima K, Ichimura E, Yasukawa Y, Wakamatsu J, Nishimura T. Dynamics of myosin replacement in skeletal muscle cells. Am J Physiol Cell Physiol 2015; 309(10): C669–79. [PubMed: 26377314]

[36]. Wolny M, Colegrave M, Colman L, White E, Knight PJ, Peckham M. Cardiomyopathy mutations in the tail of β-cardiac myosin modify the coiled-coil structure and affect integration into thick filaments in muscle sarcomeres in adult cardiomyocytes. J Biol Chem 2013; 288(44): 31952–62. [PubMed: 24047955]

[37]. da Silva Lopes K, Pietas A, Radke MH, Gotthardt M. Titin visualization in real time reveals an unexpected level of mobility within and between sarcomeres. J Cell Biol 2011; 193(4): 785–98. [PubMed: 21555460]

[38]. Cadar AG, et al. Real-time visualization of titin dynamics reveals extensive reversible photobleaching in human induced pluripotent stem cell-derived cardiomyocytes. Am J Physiol Cell Physiol 2020; 318(1): C163–C173. [PubMed: 31747312]

[39]. Wang Z, Grange M, Wagner T, Kho AL, Gautel M, Raunser S. The molecular basis for sarcomere organization in vertebrate skeletal muscle. Cell 2021; 184(8): 2135–2150. [PubMed: 33765442]

[40]. Tamborrini D, et al. In situ structures from relaxed cardiac myofibrils reveal the organization of the muscle thick filament. bioRxiv 2023; 2023.04.11.536387.

[41]. Dutta D, Nguyen V, Campbell KS, Padrón R, Craig R. Cryo-EM structure of the human cardiac myosin filament. bioRxiv 2023; 2023.04.11.536274.

[42]. Ichimura E, Ojima K, Muroya S, Kobayashi K, Nishimura T. Thick filament-associated myosin undergoes frequent replacement at the tip of the thick filament. FEBS Open Bio 2022; 12(4): 852–863.

[43]. Takahashi T, Fukukawa C, Naraoka C, Katoh T, Yazawa M. Conformations of vertebrate striated muscle myosin monomers in equilibrium with filaments. J Biochem 1999; 126(1): 34–40. [PubMed: 10393318]

[44]. Trybus KM, Huiatt TW, Lowey S. A bent monomeric conformation of myosin from smooth muscle. Proc Natl Acad Sci U S A 1982; 79(20): 6151–5. [PubMed: 6959106]

[45]. Trybus KM, Lowey S. Conformational states of smooth muscle myosin. Effects of light chain phosphorylation and ionic strength. J Biol Chem 1984; 259(13): 8564–71. [PubMed: 6610679]

[46]. Clarke J, Cota E, Fowler SB, Hamill SJ. Folding studies of immunoglobulin-like beta-sandwich proteins suggest that they share a common folding pathway. Structure 1999; 7(9): 1145–53. [PubMed: 10508783]

[47]. Politou AS, Gautel M, Pfuhl M, Labeit S, Pastore A. Immunoglobulin-type domains of titin: same fold, different stability? Biochemistry 1994; 33(15): 4730–7. [PubMed: 8161531]

[48]. Kelly CM, Manukian S, Kim E, Gage MJ. Differences in stability and calcium sensitivity of the Ig domains in titin's N2A region. Protein Sci 2020; 29(5): 1160–1171. [PubMed: 32112607]

[49]. Steward A, et al. Two immunoglobulin tandem proteins with a linking beta-strand reveal unexpected differences in cooperativity and folding pathways. J Mol Biol 2012; 416(1): 137–47. [PubMed: 22197372]

[50]. Padrón R, Dutta D, Craig R. Variants of the myosin interacting-heads motif. J Gen Physiol 2023; 155(1): e202213249. [PubMed: 36346431]

[51]. Yang S, Lee KH, Woodhead JL, Sato O, Ikebe M, Craig R. The central role of the tail in switching off 10S myosin II activity. J Gen Physiol 2019; 151(9): 1081–1093. [PubMed: 31387899]

[52]. Craig R, Smith R, Kendrick-Jones J. Light-chain phosphorylation controls the conformation of vertebrate non-muscle and smooth muscle myosin molecules. Nature 1983; 302(5907): 436–9. [PubMed: 6687627]

[53]. Milton DL, et al. Direct evidence for functional smooth muscle myosin II in the 10S self-inhibited monomeric conformation in airway smooth muscle cells. Proc Natl Acad Sci U S A 2011; 108(4): 1421–6. [PubMed: 21205888]

[54]. Bennett AM, et al. Smooth Muscle Myosin 2 Filaments Dynamically Assemble and Stabilize During Induced Contractility. bioRxiv 2022; 2022.10.10.511341.

[55]. Beach JR, Shao L, Remmert K, Li D, Betzig E, Hammer JA 3rd. Nonmuscle Myosin II Isoforms Coassemble in Living Cells. Current Biology 2014; 24(10): 1160–1166. [PubMed: 24814144]

Highlights

- Cardiac myosin molecules are highly organized within large macromolecular complexes.
- This organization appears to be highly dynamic in intact adult mouse myocardium.
- Individual molecules adopt a folded configuration when dissociated from filaments.
- Myosin filaments are designed to allow for the exchange of their components.

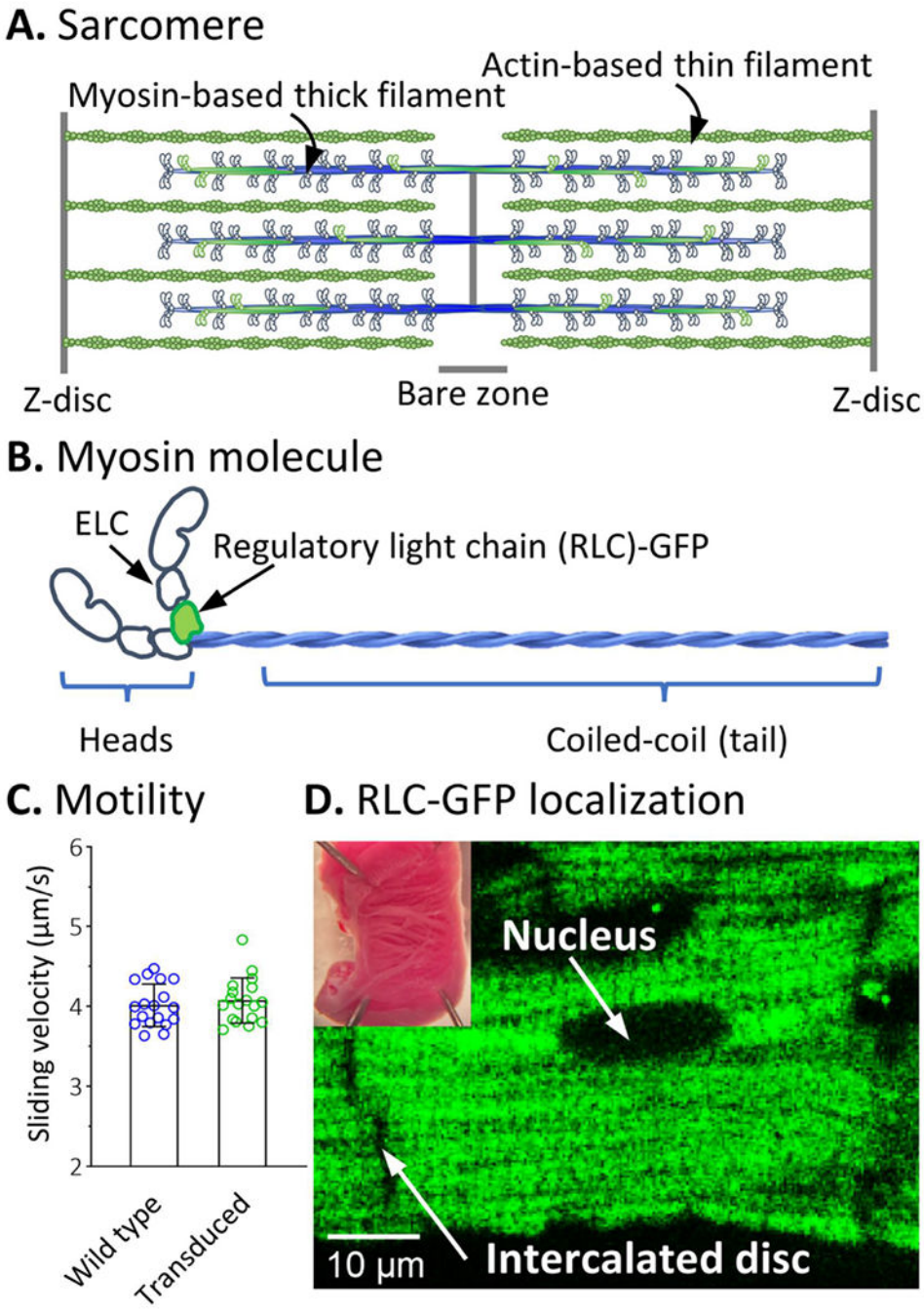

Fig. 1.

Organization and characterization of GFP-labeled RLC in the heart. (A) Illustration of the organization of myosin molecules within thick filaments in a sarcomere. (B) Illustration of a single cardiac myosin molecule, containing two heads and a long coiled-coil tail. Localization of the essential (ELC) and regulatory (RLC) light chains indicated. (C) Average velocities ± SD of actin filaments sliding on myosin isolated from hearts of FVB wild type and AAV-transduced mice in an *in vitro* motility assay. (D) RLC-GFP fluorescence observed within cardiomyocytes in an intact *ex vivo* heart preparation using two-photon microscopy.

Pixel size=1.2 x 1.2 μm, brightness and contrast were adjusted. Inset is an image of the *ex vivo* heart preparation used for imaging.

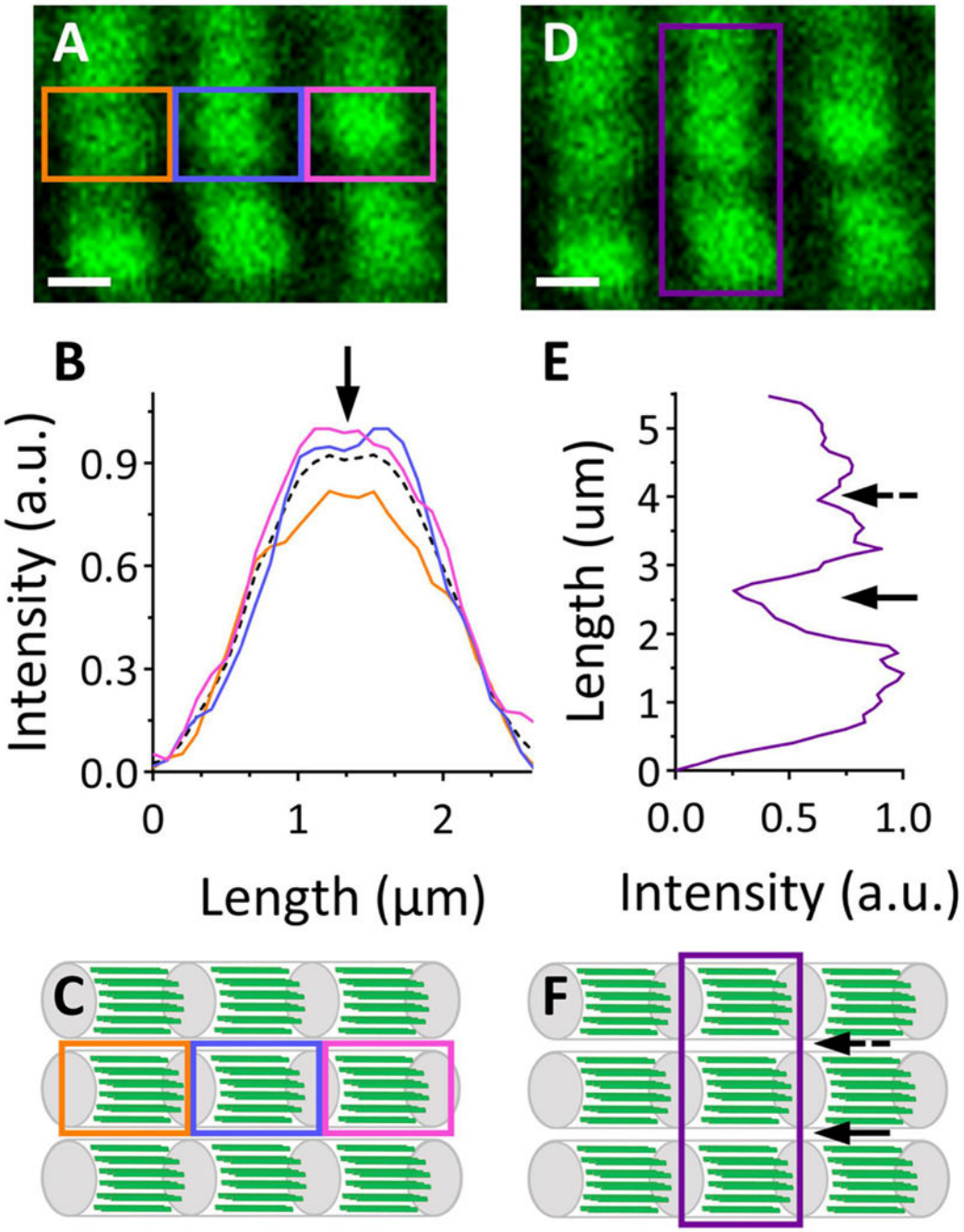

Fig. 2.

Localization of RLC-GFP within single sarcomeres. (A) RLC-GFP observed in striations with high magnification (102.5 x 102.5 nm per pixel). Three regions of interest (ROIs) shown. Scale bar is 1 μm. (B) Fluorescence-intensity distribution profiles along the x-axes of the ROIs in A. Dashed line is the average intensity. Arrow indicates a dip in fluorescence intensity in the center. (C) Illustrative model of A. (D) The same image as A, with ROI for E. (E) Fluorescence-intensity distribution profile along the y-axis of the ROI in D. Arrows

indicate dips in fluorescence intensity between myofibrils. (F) Illustrative model of D. Note: the brightness and contrast of the images in A and D were adjusted.

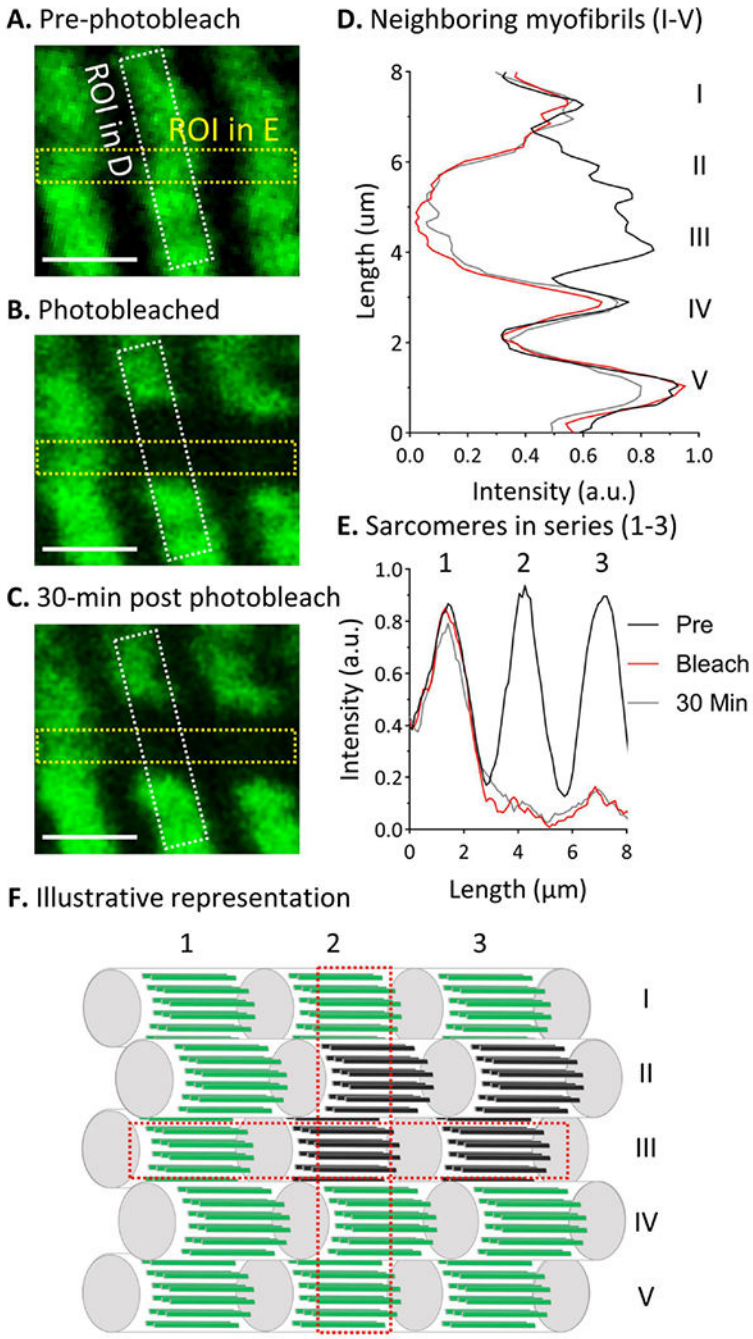

Fig. 3.

Photobleaching the entire volume of a sarcomere inhibits fluorescence recovery. Fluorescence images collected (A) prior to, (B) immediately after, and (C) 30-minutes after photobleaching the entire contents of multiple sarcomeres. Dashed boxes indicate the regions of interest (ROIs) for D and E. Scale bars are 2 µm. (D) Fluorescence-intensity distribution profile (smoothed with 3-pt moving average) along the y-axis of the yellow ROI in A-C, being indicative of five myofibrils in parallel. (E) Fluorescence-intensity distribution profile (smoothed with 3-pt moving average) along the x-axis of the white ROI in A-C,

being indicative of three sarcomeres in series within a myofibril. (F) Illustrative model to represent A-E. ROIs are indicated by dashed boxes. Sarcomeres 2 and 3 within myofibrils III and IV have been photobleached and no fluorescence recovery is observed within 30 minutes. Note: the brightness and contrast of the images in A-C were adjusted.

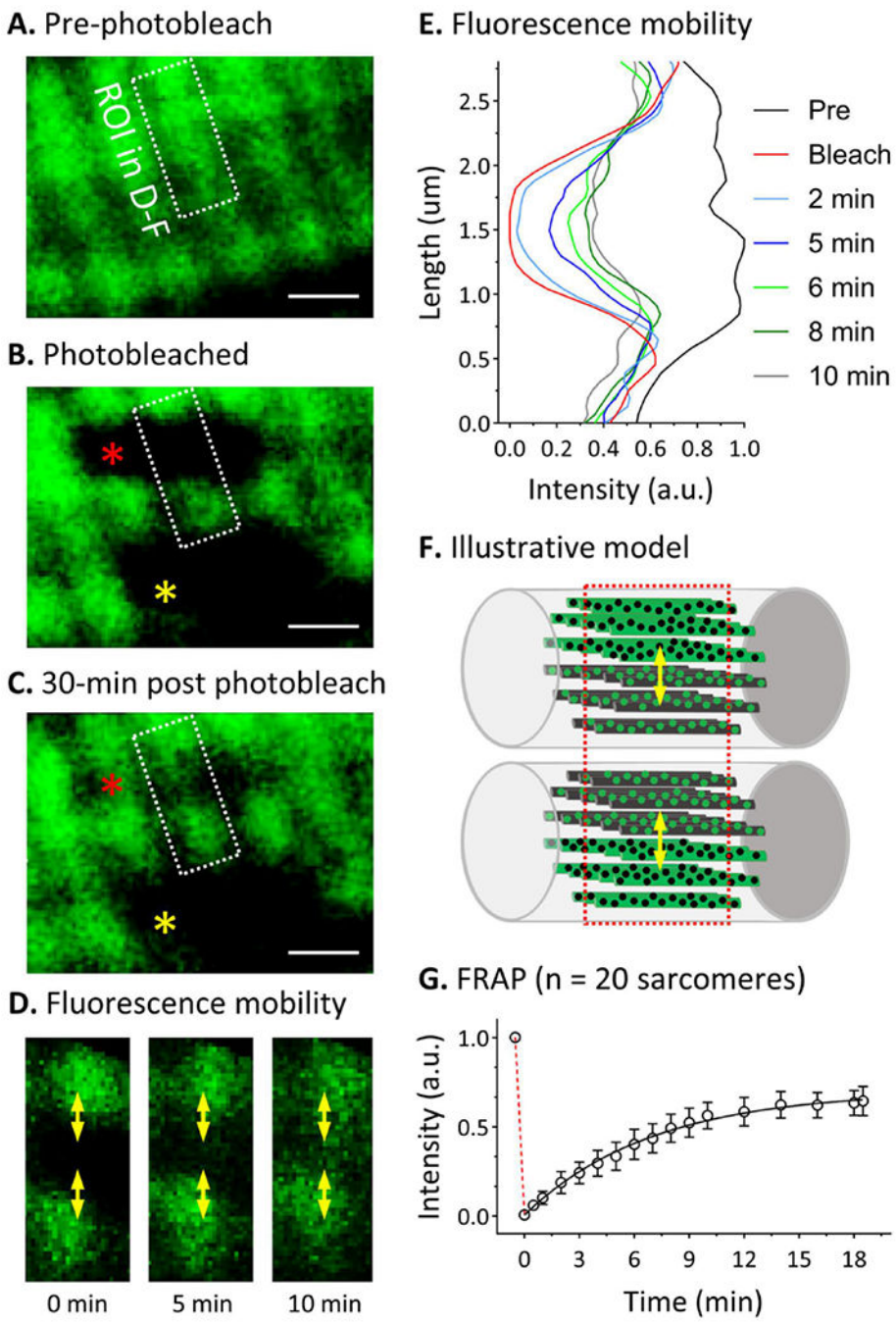

Fig. 4.

Rapid fluorescence recovery occurs when photobleaching a portion of a single sarcomere. Two-photon images taken (A) prior to, (B) immediately after, and (C) 15 minutes after photobleaching two different regions within a cardiac muscle cell in a papillary muscle (photobleached regions indicated with red and yellow asterisks in B and C). Regions of interest (ROIs) for D-F shown. Scale bars are 2 μm. (D) The ROI indicated in A-C contains two sarcomeres in parallel 0, 5, and 10 minutes after photobleaching. The red arrows indicate the redistribution of localization of the bleached and unbleached fluorescent

molecules within these sarcomeres. (E) Fluorescence-intensity distribution profile along the y-axis of the ROI shown in A-D (smoothed with 3-pt moving average). (F) Illustrative model of the redistribution of molecules within the ROI. ROI is indicated by dashed box. (F) Average fluorescence intensity ± SEM versus time for 20 sarcomeres, fitted with a single exponential. Red dashed line indicates the change in fluorescence prior to and immediately after photobleaching. Note: the brightness and contrast of the images in A-D were adjusted.

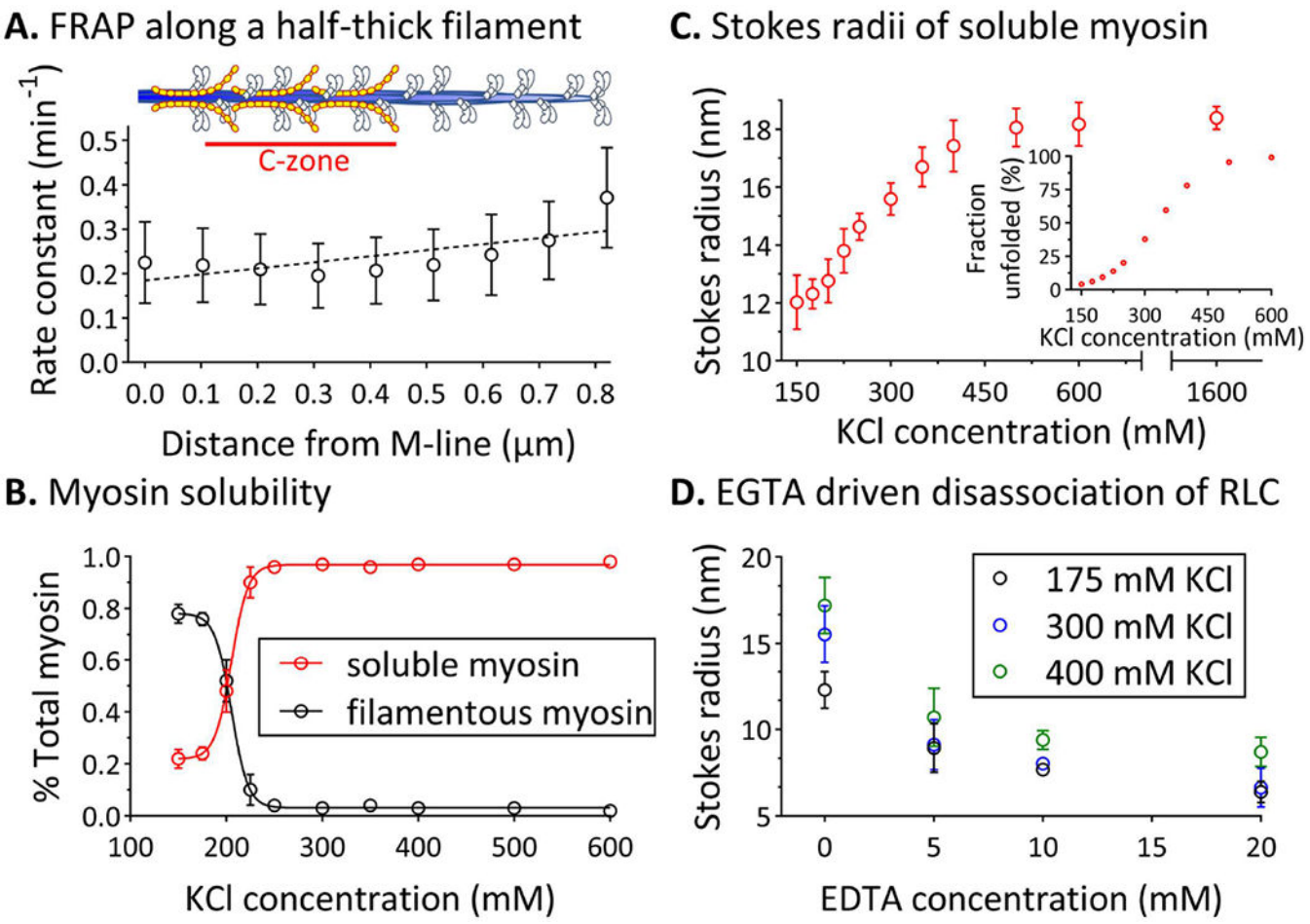

Fig. 5.

Quantification of RLC-GFP dynamics within thick filaments and whole myosin molecules. A) The rate constant of FRAP within ~100 nm regions across the length of a half-thick filament as illustrated. Dashed line is the fit of a linear regression to all the rate constants. (B) Impact of ionic strength of the fraction of RLC, ELC and myosin heavy chain organized in filaments. Average abundances ± SEM were fitted with sigmoidal equilibrium curves. (C) Average hydrodynamic radius ± SEM of RLC-GFP across a range of potassium chloride concentrations. Inset - fraction of whole myosin molecules estimated to be the extended confirmation by fitting with Eq. 3 (D) Average hydrodynamic radius ± SEM for RLC-GFP at 175, 300, 400 mM potassium chloride across EDTA concentrations.